

Monolayer V_2MX_4 : A New Family of Quantum Anomalous Hall Insulators

Yadong Jiang,¹ Huan Wang,¹ Kejie Bao,¹ Zhaochen Liu,¹ and Jing Wang^{1,2,3,*}

¹State Key Laboratory of Surface Physics and Department of Physics, Fudan University, Shanghai 200433, China

²Institute for Nanoelectronic Devices and Quantum Computing,

Zhangjiang Fudan International Innovation Center, Fudan University, Shanghai 200433, China

³Hefei National Laboratory, Hefei 230088, China

(Dated: February 13, 2024)

We theoretically propose that the van der Waals layered ternary transition metal chalcogenide V_2MX_4 ($M = W, Mo$; $X = S, Se$) is a new family of quantum anomalous Hall insulators with sizable bulk gap and Chern number $\mathcal{C} = -1$. The large topological gap originates from the *deep* band inversion between spin up bands contributed by d_{xz}, d_{yz} orbitals of V and spin down band from d_{z^2} orbital of M at Fermi level. Remarkably, the Curie temperature of monolayer V_2MX_4 is predicted to be much higher than that of monolayer $MnBi_2Te_4$. Furthermore, the thickness dependence of the Chern number for few multilayers shows interesting oscillating behavior. The general physics from the *d*-orbitals here applies to a large class of ternary transition metal chalcogenide such as Ti_2WX_4 with the space group $P-42m$. These interesting predictions, if realized experimentally, could greatly promote the research and application of topological quantum physics.

Introduction. The discovery of the quantum anomalous Hall (QAH) effect set a remarkable example for understanding topological states of quantum matter in condensed matter physics and material science [1–6]. Such a state is characterized by a topologically nontrivial insulating bulk with a finite Chern number \mathcal{C} [7, 8] but gapless chiral edge states, which is promising for the realization of dissipationless electronic devices [9, 10] and topological computation [11–13]. The QAH effect has been observed first in magnetically doped topological insulators (TI) [14–18], and subsequently in the intrinsic magnetic TI $MnBi_2Te_4$ [19], in the moiré graphene [20] and moiré transition metal dichalcogenide [21], but only at low temperature (below 5 K). Such low critical temperature is a weighty obstacle for practical applications, for example the quantum resistance standard [22]. Seeking new QAH insulator materials [23–29] with preferably large bulk gaps has become an important goal in topological material research.

Physically, the basic mechanism for the QAH effect is band inversion of the spin polarized bands [30], where both the spin-orbit coupling (SOC) and ferromagnetism are sufficiently strong. From the materials perspective, strong SOC prefers heavy elements, while the ferromagnetism favors transition metal elements preferably with 3*d* electrons. Thus the challenge in searching for large-gap QAH insulator materials is to synergize the seemingly conflicting requirement of SOC and ferromagnetism. Indeed, the inhomogeneities in magnetic TI [31–35] from magnetic dopants [36] and defects [37] drastically suppress the exchange gap by several order of magnitude, which fundamentally limits the exactly quantized anomalous Hall effect to very low temperatures. Therefore, finding stoichiometric 2D magnetic materials for QAH effect preferably in monolayer with versatile tunability is highly desired.

Here we predict a series of large-gap QAH insula-

tors in monolayer V_2MX_4 ($M = W, Mo$; $X = S, Se$), based on density functional theory (DFT) calculations and tight-binding model. The Vienna *ab initio* simulation package [45] is employed by using the Perdew-Burke-Ernzerhof [46] generalized-gradient approximation. We perform DFT + Hubbard U calculations [47]. The predicted topology was further verified by Heyd-Scuseria-Ernzerhof (HSE) hybrid functional with band gap listed in Table I [48]. These materials have the ferromagnetic (FM) ground state with Chern number $\mathcal{C} = -1$ and extraordinarily large bulk gaps (~ 0.2 eV). We find the

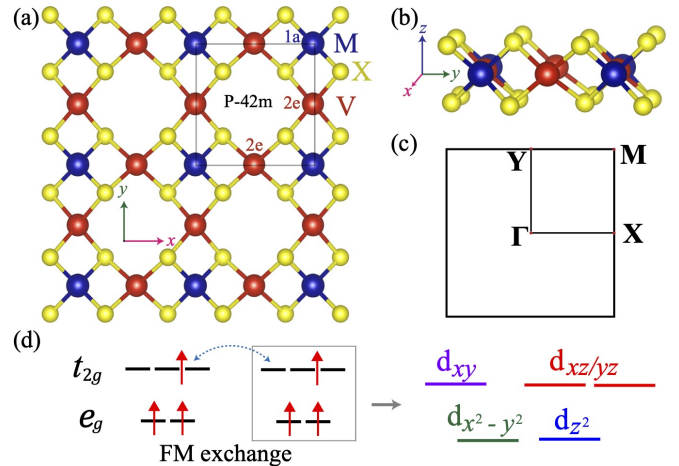


FIG. 1. (a),(b) Atomic structure of monolayer V_2MX_4 from top and side views. The Wyckoff positions 1a and 2e are displayed (notation adopted from Bilbao Crystallographic Server [38–44]). The magnetic ground state of the 2D materials class is FM along z direction with spin magnetic moment $2.6\mu_B$ per V atom. The key symmetry operations of $P-42m$ include S_{4z} , C_{2x} and C_{2z} rotations, where $S_{4z} \equiv \mathcal{I}C_{4z}$ and \mathcal{I} is inversion symmetry. (c) Brillouin zone. (d) Crystal field splitting and schematic diagram of the FM kinetic exchange coupling between the V atoms.

Materials	a (Å)	T_c (K)	E_{MAE} (meV)	E_g (meV)
V_2WS_4	5.74	470	12.1	279
V_2WSe_4	5.82	440	13.2	258
V_2MoS_4	5.72	310	2.0	115
V_2MoSe_4	5.83	284	2.2	70
Ti_2WS_4	5.75	240	10.7	259
Ti_2WSe_4	5.79	210	13.7	275

TABLE I. Lattice constant; Magnetocrystalline anisotropy energy (MAE) per unit cell E_{MAE} , defined as the total energy difference between in-plane and out-of-plane spin configurations; Curie temperature T_c from Monte Carlo simulations; Band gap E_g by using HSE method.

large topological gap originates from the deep band inversion between V d_{xz}, d_{yz} orbitals and M d_{z^2} orbital. The rich choice of candidate materials in Table I indicates that the physics here is generic with the space group $P-42m$.

Structure and magnetic properties. The monolayer V_2MX_4 has a tetragonal lattice with the space group $P-42m$ (No. 111). As shown in Fig. 1(a), each primitive cell includes three (i.e., one V_2M and two X_2) atomic layers, where each V or M atom is surrounded by four X atoms forming a distorted edge-sharing tetrahedron. These QAH materials are obtained from high-throughput screening of insulating V_2MX_4 with M from group 5 and 6, and X from group 16. Their lattice constants are listed in Table I. The dynamical and thermal stability of monolayer V_2MX_4 are confirmed by first-principles phonon and molecular dynamics calculations [49], respectively. We will mainly discuss V_2WS_4 with similar results for other materials in this class. In reality, Cu_2MX_4 and Ag_2MX_4 with the same structure have been experimentally synthesized [50–55], which implies high probability to fabricate V_2MX_4 . Meanwhile, the van der Waals nature of these materials implies the experimental feasibility to exfoliate monolayer from bulk sample.

First-principles calculations show V_2MX_4 listed in Table I have strong FM ground state with an out-of-plane easy axis [49]. The underlying mechanism of FM can be elucidated from orbital occupation. The magnetic moments are mainly provided by V ($\approx 2.6\mu_B$) rather than W ($\approx 0.4\mu_B$). The fractional magnetic moment is due to band inversion between V d_{xz}, d_{yz} orbitals and W d_{z^2} orbital (Fig. 3(a)). Thus the magnetism is from V atoms. The tetrahedral crystal field splits V 3d orbitals into doublet $e_g(d_{x^2-y^2}, d_{z^2})$ and triplet $t_{2g}(d_{xy}, d_{xz}, d_{yz})$ orbitals (Fig. 1(d)). The energy of e_g stays lower with respect to t_{2g} , because the latter point towards the negatively charged ligands. Thus each V atom is in the $e_g^2 t_{2g}^1$ configuration with the magnetic moment of $3\mu_B$ according to the Hund's rule, which is close to the DFT calculations. The FM exchange coupling between neighboring

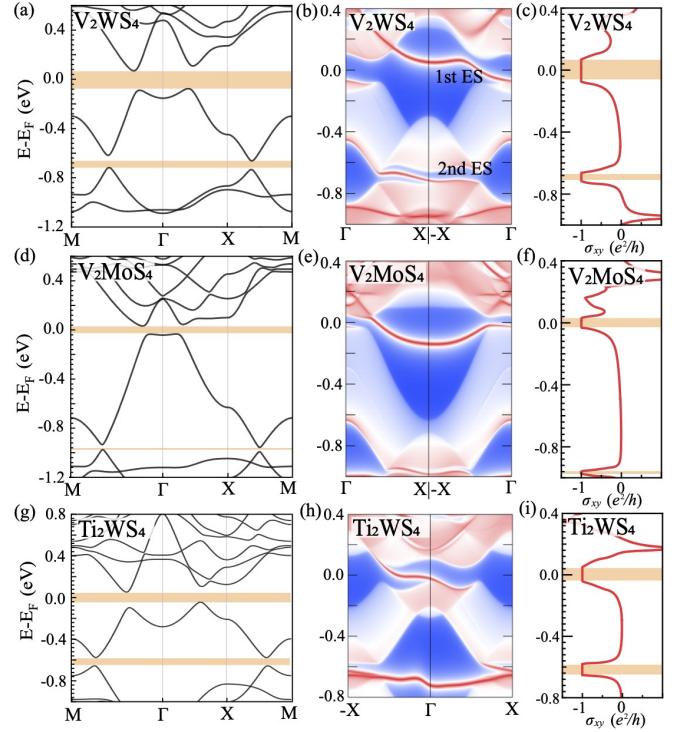


FIG. 2. Electronic structures and topological properties of monolayer V_2WS_4 , V_2MoS_4 and Ti_2WS_4 . (a)-(c) V_2WS_4 , (d)-(f) V_2MoS_4 , (g)-(i) Ti_2WS_4 . The band structure with SOC; topological edge states (ES) calculated along x axis; and anomalous Hall conductance σ_{xy} as a function of Fermi energy, respectively. The shaded regions in (a),(d),(g) denote the topological gap.

V atoms is strongly enhanced by Hund's rule interaction due to empty t_{2g} orbitals [56]. Furthermore, the predicted Curie temperature for monolayer V_2MX_4 is much higher than that of MnBi_2Te_4 .

Electronic structures. Fig. 2(a) and Fig. 3(a) display the electronic structure of monolayer V_2WS_4 with and without SOC, respectively. There are two band inversions between different spin polarized bands, both of which are further gapped by SOC. Specifically, one is near the Fermi energy E_F between spin up bands contributed by d_{xy}, d_{yz} orbitals of V and spin down band by d_{z^2} orbital of W, the other is about 0.7 eV below E_F between V d_{xy}, d_{yz} spin up bands and W $d_{x^2-y^2}$ spin down band. There also exists a spin polarized quadratic band touching at Γ point from d_{xy}, d_{yz} orbitals of V above E_F , with the nontrivial gap opened by SOC [57]. The anomalous Hall conductance σ_{xy} versus E_F is calculated in Fig. 2(c), which displays a quantized value of $-e^2/h$ near both E_F and $E_F - 0.7$ eV. This indicates the topological nontrivial bands with $\mathcal{C} = -1$ below $E_F - 0.7$ eV, which is consistent with single chiral edge states dispersing within the bulk gap as in the edge local density of states (Fig. 2(b)). Interestingly, there also exists an occupied 2nd chiral edge state which is 0.7 eV below E_F , which can be measured

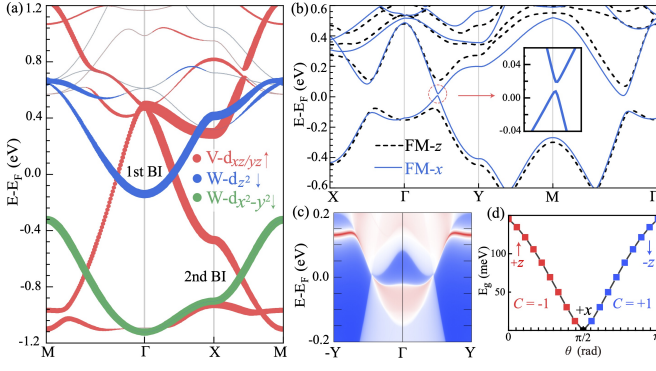


FIG. 3. (a) The d -orbitals projection band structures without SOC of monolayer V_2WS_4 , only those bands which is related to band inversion are shown. (b) The band structure for FM along z - and x -axis of V_2WS_4 with SOC. (c) Energy and momentum dependence of the edge local density of state along y -axis under FM- x state of V_2WS_4 . (d) Dependence of bulk gap along the high symmetry line and C on the spin orientation quantified by a polar angle θ , where $\theta = 0, \pi/2, \pi$ denote the $+z, +x, -z$ directions, respectively.

by scanning tunneling microscope. By replacing W by the same group element Mo, V_2MoS_4 monolayer has similar band structure and same topological properties as shown in Fig. 2(d)-2(f). The topological gap of monolayer V_2WX_4 is larger than that of V_2MoX_4 , which is due to enhanced SOC from heavier elements and deeper band inversion.

The topological gap strongly depends on spin orientations. Fig. 3(b) shows the band structure for the in-plane ferromagnetism along x -axis. The symmetries of the system reduces to C_{2x} and $C_{2x}\mathcal{T}$, where \mathcal{T} is time-reversal. One can see the gap along Γ -Y decreases but not closes, for there is no symmetry to guarantee a gapless point. Along the high symmetry lines, there is a small negative indirect gap between valence top along Γ -Y and conduction bottom along Γ -M. The Chern number of valence bands are calculated to be $C = 0$, which is guaranteed by $C_{2x}\mathcal{T}$. Similar to \mathcal{IT} , σ_{xy} is odd under $C_{2x}\mathcal{T}$ in 2D materials, which ensures $C = 0$ when ferromagnetism is completely along any in-plane direction. This is consistent with the edge local density of state calculation in Fig. 3(c), where there is no chiral edge state. The FM- x state is trivial without any kinds of topology, which is checked by the band representation of C_{2x} (i.e., symmetry indicator). Then by varying the spin orientation from $+z$ to $+x$, then to $-z$ axis, the band gap monotonically decreases to close, and negative then reopens, which is accompanied by the topological phase transitions from $C = -1$ to $C = 0$ and then to $C = 1$ in Fig. 3(d). The gap varies approximately in relation as $E_g \propto S \cos(\theta + \theta_0) \approx \langle S_z \rangle$, with $\theta_0 \approx 0.1$ [49]. This simply means the topologically nontrivial gap is opened by SOC related to $\langle S_z \rangle$ component, while the trivial gap is associated with $\langle S_x \rangle$ component.

The intimate relationship between band gap and spin orientation implies that the electronic structure is renormalized by magnon excitations. In FM- z ground state, the magnons contribution to magnetization is $\langle S_z \rangle = S - \int d^2\mathbf{k} n_B(\epsilon_{\mathbf{k}})/(2\pi)^2$, where $n_B(\epsilon_{\mathbf{k}}) \equiv 1/[\exp(\epsilon_{\mathbf{k}}/k_B T) - 1]$ is the Bose distribution, $\epsilon_{\mathbf{k}}$ is magnon dispersion. Taking V_2WS_4 as an example, $S = 3/2$ and the magnon gap is estimated to be 5.34 meV. Thus when $T < 58$ K, the magnon is absent; when $T \lesssim 200$ K, the reduction in $\langle S_z \rangle$ from magnon excitation is less than 6% compared to $\langle S_z \rangle = 3/2$ [49]. Therefore, the large topological gap of ground state still holds in the presence of magnon excitation. It is worth mentioning that when temperature is close to T_c , the significant thermal spin fluctuation will decrease $\langle S_z \rangle$ and topological gap dramatically.

Tight-binding model and origin of topology. To reveal the origin of $C = -1$ topology in the electronic structure, we perform the symmetry analysis of the band irreducible representation and construct a tight-binding model to recover the essential topological physics. The first and second band inversions occur at Γ and M point, respectively. Naively, one may simply count the angular momentum difference locally at the band inversion point to be the Chern number change as in the conventional s - p band inversion. However, this is incorrect due to band inversion from the opposite spin polarization here. For example, at M point for second band inversion, only spin contributes to the angular momentum difference, which implies the lowest band ($d_{x^2-y^2}^{\downarrow}$ from W) should have $C = 1$, this is contrary to the first principles calculations of $C = -1$.

Then we construct a concrete tight-binding model including $d_{xz}^{\uparrow}, d_{yz}^{\uparrow}$ of V and $d_{z^2}^{\downarrow}, d_{x^2-y^2}^{\downarrow}$ of W to decipher the origin of topology. There are two V in an unit cell, and d_{xz}, d_{yz} orbitals of each V are non-degenerate. However, d_{xz} of one V and d_{yz} of the other V are degenerate, which are related to each other by S_{4z} . Therefore, for the low energy physics, we only need to consider $d_{xz}^{\uparrow}, d_{yz}^{\uparrow}$ from two V, respectively and $d_{z^2}^{\downarrow}, d_{x^2-y^2}^{\downarrow}$ of W, namely a four orbitals model. The Hamiltonian is obtained by considering the nearest-neighbor and next-nearest-neighbor hopping with SOC included, where the explicit forms are in Supplementary Materials [49]. As shown in Fig. 4(a) and 4(b), the band structure and the corresponding irreducible representations of high symmetry points (listed in Table II) in DFT calculation (Fig. 2(a) and Fig. 3(a)) are rebuilt in our tight-binding model.

The symmetry generators of space group $P-42m$ are S_{4z}, C_{2z} and C_{2x} . For tight-binding model of V_2MX_4 , \mathcal{I} can be viewed as C_{2z} due to lacking of z direction. Then S_{4z} becomes C_{4z}^3 , namely, the system is effectively C_{4z} invariant. The Chern number of band in a S_4 invariant system is shown to be [49, 58],

$$i^C = \prod_{j \in \text{occupied}} (-1)^F \xi_j(\Gamma) \xi_j(M) \zeta_j(X). \quad (1)$$

Here $F = 1$ for spinful case. $\xi_j(k)$ is the eigenvalue of

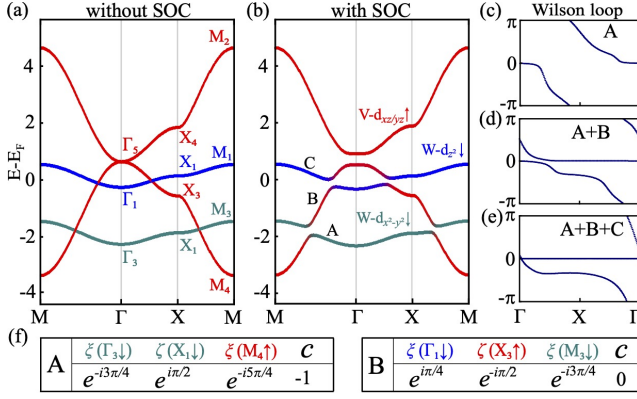


FIG. 4. (a),(b) The d -orbitals projection band structure of the tight-binding model with and without SOC. The irreducible representation at high-symmetry points of the Brillouin zone boundary and the orbital compositions (color of the bands) are consistent with that in Fig. 3(a). (c)-(e), The Wilson loop for the lowest one, two and three bands in (b), respectively. (f) Eigenvalues of S_{4z} at Γ and M points and C_{2z} at X point of bands A and B. Chern number C are calculated by Eq. (1).

S_{4z} at the S_{4z} -invariant Γ and M points of the j -th band, $\zeta_j(k)$ is the eigenvalue of C_{2z} at the C_{2z} -invariant X point on the j -th band. Now the band topology can be diagnosed by the symmetry information listed in Table II. The eigenvalues and Chern numbers for lowest (A) and second lowest band (B) are calculated in Fig. 4(f). All of these are consistent with the Wilson loop calculations for the lowest one and two bands shown in Fig. 4(c) and 4(d). The quadratic band touching at Γ_5 is from degenerate d_{xz}, d_{yz} , which have an effective angular momentum $\ell_z = \pm 1$, and SOC opens a topologically nontrivial gap [57]. Thus the Chern number summation of lowest three bands is only determined by the sign of SOC. As shown in Fig. 4(e), the total Chern number of the lowest three bands is $C = -1$, namely, both bands B and C have $C = 0$, and the only nontrivial $C = -1$ is carried by band A, which is consistent with first principles calculations. If we artificially reverse the sign of SOC, then the Chern number of the lowest three bands are $(C_A, C_B, C_C) = (-1, 0, 2)$. Now we fully understand that the topology in this system is not only from gapping the degenerate d_{xz}, d_{yz} orbitals of V by SOC, but also the band inversions from them and W d_{z^2} and $d_{x^2-y^2}$.

Here we analyze the origin of the large topological gap. The topological gap is from SOC term as $\lambda_{so} \ell \cdot \mathbf{s} = \lambda_{so}(\ell_+ s_- + \ell_- s_+)/2 + \lambda_{so} \ell_z s_z$, where λ_{so} is atomic SOC strength. The nontrivial gap is opened by combining the first term with orbital hopping and hybridization. For spin polarized band inversion in QAH, two bands are inverted at certain high-symmetry point in the Brillouin zone, and topological gap E_g opens at a finite wave vector δk away from the band inversion point due to orbital hybridization with $E_g \propto \lambda' \delta k$, where λ' is the hybridiza-

	Γ	X	M
$d_{z^2} @ 1a$	$\Gamma_1(1)$	$X_1(1)$	$M_1(1)$
$d_{x^2-y^2} @ 1a$	$\Gamma_3(1)$	$X_1(1)$	$M_3(1)$
$d_{xz, yz} @ 2e$	$\Gamma_5(2)$	$X_3(1) \oplus X_4(1)$	$M_2(1) \oplus M_4(1)$

TABLE II. Partial elementary band representations without time-reversal symmetry for space group $P-42m$.

tion strength. For spin polarized band inversion with same spin such as MnBi_2Te_4 [33, 34], $\lambda' \propto \lambda_{so}^2$, namely second-order process. In V_2MX_4 , the band inversion are between opposite spin polarized bands, $\lambda' \propto \lambda_{so}$, thus a lower-order process with greater strength in gap opening. Meanwhile, these materials have deep band inversion with large δk . Therefore, both λ' and δk are enhanced in V_2MX_4 and lead to large topological gap.

Material generalization. The key for the $C = -1$ phase here is rooted in the spin polarized quadratic band touching of d_{xz}, d_{yz} orbitals at Γ point, where S_{4z} ensures their degeneracy. With SOC and certain orbital occupations, QAH phase can be realized. In fact, the model and analysis from d orbitals above are quite general, and also apply to monolayer Ti_2WX_4 ($X = \text{S}, \text{Se}$) with the same lattice structure of $P-42m$ symmetry and similar d -orbital projected band structure and irreducible representations [49]. Ti_2WX_4 has the FM ground state, and the magnetism is from Ti atom. Interestingly, the bandwidth of d_{z^2} orbital is much narrower than that of d_{xz}, d_{yz} orbitals in Ti. Each Ti atom is in the $e_g^1 t_{2g}^1$ configuration with the magnetic moment close to $2\mu_B$ according to the Hund's rule. The e_g - t_{2g} kinetic exchange leads to strong ferromagnetism [29]. Meanwhile, similar two band inversions occur between $d_{xy}^\uparrow, d_{yz}^\uparrow$ bands of Ti and $d_{z^2}^\downarrow$ band of W first at E_F , and $d_{x^2-y^2}^\downarrow$ band of W then below E_F . By adding SOC, the nontrivial topology from quadratic band touching of d_{xz}, d_{yz} at Γ is now transmitted to the bands below E_F , leading to the $C = -1$ QAH phase (Fig. 2(g)-(i)). We point out that Ti d -orbitals contribute both of topology and magnetism, nevertheless the physics is quite different from KTiSb class of compounds, where the topology is from band inversion from d_{xz}, d_{yz} and d_{z^2} at M point [29].

Discussions. The topological band structures in these materials have interesting thickness dependence. Bilayer V_2WS_4 has AA or AB stacking. The magnetic ground state is A-type AFM with the out-of-plane easy axis in AB stacking, which is FM within each layer but AFM between the adjacent layer. The t_{2g} - t_{2g} exchange of V atoms between neighbor layers via p orbitals of ligand is AFM due to Goodenough-Kanamori-Anderson rule [56]. The system has a full band gap and gapped helical edge state, namely $C = 0$, which can be simply viewed as stacking of two QAH with opposite Chern number along

z -axis. The FM- z state of bilayer also has a full gap but with $\mathcal{C} = -2$. We further calculate the trilayer case and obtain AFM ground state with an uncompensated FM layer along z axis, and the system is a $\mathcal{C} = -1$ QAH insulator [49]. Therefore, we expect \mathcal{C} will oscillate between -1 and 0 depending on odd and even layers of multilayer, as long as it has a full band gap.

The quantized σ_{xy} and vanishing longitudinal conductivity of QAH insulator imply a quantized Kerr/Faraday rotation [59, 60], when the frequency satisfies $\omega \ll E_g/\hbar$. However, such a quantized magnetooptical effect has not been achieved in existing QAH systems yet due to the small band gap [61, 62]. Here the topologically nontrivial Chern bands in V_2MX_4 lies far below and above E_F , which provides an intriguing but rare platform for exploring giant Kerr rotation from the optical transitions between Chern bands, even possibly in the optical frequency range.

In summary, our work uncover large gap $\mathcal{C} = -1$ QAH phase with interesting interplay between magnetism and topology solely from d orbitals, which applies to a large class of ternary chalcogenide in space group $P-42m$. The rich choice of candidate materials indicate the physics is quite general. We hope the theoretical work here could aid the search for new QAH insulators in transition metal compounds.

Acknowledgment. This work is supported by the National Key Research Program of China under Grant No. 2019YFA0308404, the Natural Science Foundation of China through Grants No. 12350404 and No. 12174066, the Innovation Program for Quantum Science and Technology through Grant No. 2021ZD0302600, the Science and Technology Commission of Shanghai Municipality under Grants No. 23JC1400600 and No. 20JC1415900, Shanghai Municipal Science and Technology Major Project under Grant No. 2019SHZDZX01. Y.J. and H.W. contributed equally to this work.

* Corresponding author: wjingphys@fudan.edu.cn

- [1] M. Z. Hasan and C. L. Kane, “Colloquium: Topological insulators,” *Rev. Mod. Phys.* **82**, 3045–3067 (2010).
- [2] Xiao-Liang Qi and Shou-Cheng Zhang, “Topological insulators and superconductors,” *Rev. Mod. Phys.* **83**, 1057–1110 (2011).
- [3] Yoshinori Tokura, Kenji Yasuda, and Atsushi Tsukazaki, “Magnetic topological insulators,” *Nature Rev. Phys.* **1**, 126–143 (2019).
- [4] Jing Wang and Shou-Cheng Zhang, “Topological states of condensed matter,” *Nature Mat.* **16**, 1062–1067 (2017).
- [5] B. Andrei Bernevig, Claudia Felser, and Haim Beidenkopf, “Progress and prospects in magnetic topological materials,” *Nature* **603**, 41–51 (2022).
- [6] Cui-Zu Chang, Chao-Xing Liu, and Allan H. MacDonald, “Colloquium: Quantum anomalous hall effect,” *Rev. Mod. Phys.* **95**, 011002 (2023).
- [7] D. J. Thouless, M. Kohmoto, M. P. Nightingale, and M. den Nijs, “Quantized hall conductance in a two-dimensional periodic potential,” *Phys. Rev. Lett.* **49**, 405–408 (1982).
- [8] F. D. M. Haldane, “Model for a quantum hall effect without landau levels: Condensed-matter realization of the “parity anomaly,”” *Phys. Rev. Lett.* **61**, 2015–2018 (1988).
- [9] Xiao Zhang and Shou-Cheng Zhang, “Chiral interconnects based on topological insulators,” *Proc. SPIE Micro- and Nanotechnology Sensors, Systems, and Applications IV* **8373**, 837309 (2012).
- [10] Jing Wang, Biao Lian, Haijun Zhang, Yong Xu, and Shou-Cheng Zhang, “Quantum anomalous hall effect with higher plateaus,” *Phys. Rev. Lett.* **111**, 136801 (2013).
- [11] Xiao-Liang Qi, Taylor L. Hughes, and Shou-Cheng Zhang, “Chiral topological superconductor from the quantum hall state,” *Phys. Rev. B* **82**, 184516 (2010).
- [12] Jing Wang, Quan Zhou, Biao Lian, and Shou-Cheng Zhang, “Chiral topological superconductor and half-integer conductance plateau from quantum anomalous hall plateau transition,” *Phys. Rev. B* **92**, 064520 (2015).
- [13] Biao Lian, Xiao-Qi Sun, Abolhassan Vaezi, Xiao-Liang Qi, and Shou-Cheng Zhang, “Topological quantum computation based on chiral majorana fermions,” *Proc. Natl. Acad. Sci. USA* **115**, 10938–10942 (2018).
- [14] Cui-Zu Chang, Jinsong Zhang, Xiao Feng, Jie Shen, Zuo-cheng Zhang, Minghua Guo, Kang Li, Yunbo Ou, Pang Wei, Li-Li Wang, Zhong-Qing Ji, Yang Feng, Shuai-hua Ji, Xi Chen, Jinfeng Jia, Xi Dai, Zhong Fang, Shou-Cheng Zhang, Ke He, Yayu Wang, Li Lu, Xu-Cun Ma, and Qi-Kun Xue, “Experimental Observation of the Quantum Anomalous Hall Effect in a Magnetic Topological Insulator,” *Science* **340**, 167–170 (2013).
- [15] Cui-Zu Chang, Weiwei Zhao, Duk Y. Kim, Haijun Zhang, Badih A. Assaf, Don Heiman, Shou-Cheng Zhang, Chaoxing Liu, Moses H. W. Chan, and Jagadeesh S. Moodera, “High-precision realization of robust quantum anomalous hall state in a hard ferromagnetic topological insulator,” *Nature Mater.* **14**, 473 (2015).
- [16] M. Mogi, R. Yoshimi, A. Tsukazaki, K. Yasuda, Y. Kozuka, K. S. Takahashi, M. Kawasaki, and Y. Tokura, “Magnetic modulation doping in topological insulators toward higher-temperature quantum anomalous hall effect,” *Appl. Phys. Lett.* **107**, 182401 (2015).
- [17] A. J. Bestwick, E. J. Fox, Xufeng Kou, Lei Pan, Kang L. Wang, and D. Goldhaber-Gordon, “Precise quantization of the anomalous hall effect near zero magnetic field,” *Phys. Rev. Lett.* **114**, 187201 (2015).
- [18] R. Watanabe, R. Yoshimi, M. Kawamura, M. Mogi, A. Tsukazaki, X. Z. Yu, K. Nakajima, K. S. Takahashi, M. Kawasaki, and Y. Tokura, “Quantum anomalous hall effect driven by magnetic proximity coupling in all-telluride based heterostructure,” *Appl. Phys. Lett.* **115**, 102403 (2019).
- [19] Yujun Deng, Yijun Yu, Meng Zhu Shi, Zhongxun Guo, Zihan Xu, Jing Wang, Xian Hui Chen, and Yuanbo Zhang, “Quantum anomalous hall effect in intrinsic magnetic topological insulator mnb2te4,” *Science* **367**, 895–900 (2020).
- [20] M. Serlin, C. L. Tschirhart, H. Polshyn, Y. Zhang, J. Zhu, K. Watanabe, T. Taniguchi, L. Balents, and A. F.

- Young, “Intrinsic quantized anomalous hall effect in a moiré heterostructure,” *Science* **367**, 900–903 (2020).
- [21] Tingxin Li, Shengwei Jiang, Bowen Shen, Yang Zhang, Lizhong Li, Zui Tao, Trithep Devakul, Kenji Watanabe, Takashi Taniguchi, Liang Fu, Jie Shan, and Kin Fai Mak, “Quantum anomalous hall effect from intertwined moiré bands,” *Nature* **600**, 641–646 (2021).
- [22] Yuma Okazaki, Takehiko Oe, Minoru Kawamura, Ryutaro Yoshimi, Shuji Nakamura, Shintaro Takada, Masataka Mogi, Kei S. Takahashi, Atsushi Tsukazaki, Masashi Kawasaki, Yoshinori Tokura, and Nobu-Hisa Kaneko, “Quantum anomalous hall effect with a permanent magnet defines a quantum resistance standard,” *Nature Phys.* **18**, 25–29 (2022).
- [23] Jing-Yang You, Zhen Zhang, Bo Gu, and Gang Su, “Two-dimensional room-temperature ferromagnetic semiconductors with quantum anomalous hall effect,” *Phys. Rev. Applied* **12**, 024063 (2019).
- [24] Jiaxiang Sun, Xin Zhong, Wenwen Cui, Jingming Shi, Jian Hao, Meiling Xu, and Yinwei Li, “The intrinsic magnetism, quantum anomalous hall effect and curie temperature in 2d transition metal trihalides,” *Phys. Chem. Chem. Phys.* **22**, 2429–2436 (2020).
- [25] Yang Li, Jiaheng Li, Yang Li, Meng Ye, Fawei Zheng, Zetao Zhang, Jingheng Fu, Wenhui Duan, and Yong Xu, “High-temperature quantum anomalous hall insulators in lithium-decorated iron-based superconductor materials,” *Phys. Rev. Lett.* **125**, 086401 (2020).
- [26] X. Xuan, Z. Zhang, C. Chen, and W. Guo, “Robust quantum anomalous hall states in monolayer and few-layer tite,” *Nano Lett.* **22**, 5379–5384 (2022).
- [27] Qilong Sun, Yandong Ma, and Nicholas Kioussis, “Two-dimensional dirac spin-gapless semiconductors with tunable perpendicular magnetic anisotropy and a robust quantum anomalous hall effect,” *Mater. Horiz* **7**, 2071–2077 (2020).
- [28] Zeyu Li, Yulei Han, and Zhenhua Qiao, “Chern number tunable quantum anomalous hall effect in monolayer transitional metal oxides via manipulating magnetization orientation,” *Phys. Rev. Lett.* **129**, 036801 (2022).
- [29] Yadong Jiang, Huan Wang, and Jing Wang, “Large-gap quantum anomalous hall insulators in the $a\text{Tix}$ ($a = \text{K, rb, sr}; x = \text{sb, bi, sn}$) class of compounds,” *Phys. Rev. B* **108**, 165122 (2023).
- [30] Chao-Xing Liu, Xiao-Liang Qi, Xi Dai, Zhong Fang, and Shou-Cheng Zhang, “Quantum anomalous hall effect in $\text{Hg}_{1-y}\text{Mn}_y\text{Te}$ quantum wells,” *Phys. Rev. Lett.* **101**, 146802 (2008).
- [31] Rui Yu, Wei Zhang, Hai-Jun Zhang, Shou-Cheng Zhang, Xi Dai, and Zhong Fang, “Quantized Anomalous Hall Effect in Magnetic Topological Insulators,” *Science* **329**, 61–64 (2010).
- [32] Jing Wang, Biao Lian, and Shou-Cheng Zhang, “Quantum anomalous hall effect in magnetic topological insulators,” *Phys. Scr.* **T164**, 014003 (2015).
- [33] Dongqin Zhang, Minji Shi, Tongshuai Zhu, Dingyu Xing, Haijun Zhang, and Jing Wang, “Topological axion states in the magnetic insulator mnbi_2te_4 with the quantized magnetoelectric effect,” *Phys. Rev. Lett.* **122**, 206401 (2019).
- [34] Jiaheng Li, Yang Li, Shiqiao Du, Zun Wang, Bing-Lin Gu, Shou-Cheng Zhang, Ke He, Wenhui Duan, and Yong Xu, “Intrinsic magnetic topological insulators in van der waals layered mnbi_2te_4 -family materials,” *Sci. Adv.* **5**, eaaw5685 (2019).
- [35] M. M. Otrokov, I. P. Rusinov, M. Blanco-Rey, M. Hoffmann, A. Yu. Vyazovskaya, S. V. Eremeev, A. Ernst, P. M. Echenique, A. Arnau, and E. V. Chulkov, “Unique thickness-dependent properties of the van der waals interlayer antiferromagnet mnbi_2te_4 films,” *Phys. Rev. Lett.* **122**, 107202 (2019).
- [36] Yi Xue Chong, Xiaolong Liu, Rahul Sharma, Andrey Kostin, Genda Gu, K. Fujita, J. C. Séamus Davis, and Peter O. Sprau, “Severe dirac mass gap suppression in sb_2te_3 -based quantum anomalous hall materials,” *Nano Lett.* **20**, 8001–8007 (2020).
- [37] M. Garnica, M. M. Otrokov, P. Casado Aguilar, I. I. Klimovskikh, D. Estyunin, Z. S. Aliev, I. R. Amiraslanov, N. A. Abdullayev, V. N. Zverev, M. B. Babanly, N. T. Mamedov, A. M. Shikin, A. Arnau, A. L. Vázquez de Parga, E. V. Chulkov, and R. Miranda, “Native point defects and their implications for the dirac point gap at $\text{mnbi}_2\text{te}_4(0001)$,” *npj Quantum Mater.* **7**, 7 (2022).
- [38] M I Aroyo, J M Perezmato, C Capillas, E Kroumova, Svetoslav Ivantchev, G Madariaga, A Kirov, and Hans Wondratschek, “Bilbao crystallographic server: I. databases and crystallographic computing programs,” *Z. Krist.* **221**, 15–27 (2006).
- [39] Asen Kirov, Cesar Capillas, J Perez-Mato, and Hans Wondratschek, “Bilbao crystallographic server. ii. representations of crystallographic point groups and space groups,” *Acta Cryst.* **62**, 115–28 (2006).
- [40] J. Perez-Mato, D Orobengoa, Emre Tasci, Gemma De la Flor Martin, and A Kirov, “Crystallography online: Bilbao crystallographic server,” *Bulg. Chem. Commun.* **43**, 183–197 (2011).
- [41] Jorrit Kruthoff, Jan de Boer, Jasper van Wezel, Charles L. Kane, and Robert-Jan Slager, “Topological classification of crystalline insulators through band structure combinatorics,” *Phys. Rev. X* **7**, 041069 (2017).
- [42] M. G. Vergniory, L. Elcoro, Zhijun Wang, Jennifer Cano, C. Felser, M. I. Aroyo, B. Andrei Bernevig, and Barry Bradlyn, “Graph theory data for topological quantum chemistry,” *Phys. Rev. E* **96**, 023310 (2017).
- [43] L. Elcoro, Barry Bradlyn, Z. Wang, M. G. Vergniory, Jennifer Cano, C. Felser, B. Bernevig, D. Orobengoa, G. D. L. Flor, and M. Aroyo, “Double crystallographic groups and their representations on the bilbao crystallographic server,” *J. Appl. Crystallogr* **50**, 1457 (2017).
- [44] Barry Bradlyn, L Elcoro, Jennifer Cano, MG Vergniory, Zhijun Wang, C Felser, MI Aroyo, and B Andrei Bernevig, “Topological quantum chemistry,” *Nature* **547**, 298 (2017).
- [45] G. Kresse and J. Furthmüller, “Efficient iterative schemes for ab initio total-energy calculations using a plane-wave basis set,” *Phys. Rev. B* **54**, 11169–11186 (1996).
- [46] John P. Perdew, Kieron Burke, and Matthias Ernzerhof, “Generalized gradient approximation made simple,” *Phys. Rev. Lett.* **77**, 3865–3868 (1996).
- [47] S. L. Dudarev, G. A. Botton, S. Y. Savrasov, C. J. Humphreys, and A. P. Sutton, “Electron-energy-loss spectra and the structural stability of nickel oxide: An lsda+u study,” *Phys. Rev. B* **57**, 1505–1509 (1998).
- [48] Aliaksandr V. Krukau, Oleg A. Vydrov, Artur F. Izmaylov, and Gustavo E. Scuseria, “Influence of the exchange screening parameter on the performance of screened hybrid functionals,” *J. Chem. Phys* **125**, 224106 (2006).

- [49] See Supplementary Material at [url], for technical details on methods of first-principles calculation, stability and magnetic ground state, electronic structure and orbital projection, Ti_2MoX_4 and V_2TaX_4 family, bilayer and trilayer V_2WS_4 , and theory, which includes Refs. [63–79].
- [50] Clare J. Crossland, Peter J. Hickey, and John S. O. Evans, “The synthesis and characterisation of Cu_2MX_4 ($m = \text{w}$ or mo ; $x = \text{s}$, se or s/se) materials prepared by a solvothermal method,” *J. Mater. Chem.* **15**, 3452–3458 (2005).
- [51] Li-Yong Gan and Udo Schwingenschlögl, “Two-dimensional square ternary Cu_2MX_4 ($m = \text{mo}$, w ; $x = \text{s}$, se) monolayers and nanoribbons predicted from density functional theory,” *Phys. Rev. B* **89**, 125423 (2014).
- [52] Xin Hu, Wei Shao, Xudong Hang, Xiaodong Zhang, Wenguang Zhu, and Yi Xie, “Superior electrical conductivity in hydrogenated layered ternary chalcogenide nanosheets for flexible all-solid-state supercapacitors,” *Angew. Chem. Int. Ed.* **55**, 5733–5738 (2016).
- [53] Fengping Zhan, Qinghua Wang, Yibing Li, Xin Bo, Qingxiang Wang, Fei Gao, and Chuan Zhao, “Low-temperature synthesis of cuboid silver tetrathiotungstate (Ag_2WS_4) as electrocatalyst for hydrogen evolution reaction,” *Inorg. Chem.* **57**, 5791–5800 (2018).
- [54] Qian Wu, Yandong Ma, Rui Peng, Baibiao Huang, and Ying Dai, “Single-layer Cu_2WS_4 with promising electrocatalytic activity toward hydrogen evolution reaction,” *ACS Appl. Mater. Interfaces* **11**, 45818–45824 (2019).
- [55] Yunxiang Lin, Shuangming Chen, Ke Zhang, and Li Song, “Recent advance of ternary layered Cu_2MX_4 ($m = \text{mo}$, w ; $x = \text{s}$, se) nanomaterials for photocatalysis,” *Solar RRL* **3**, 1800320 (2019).
- [56] Daniel I. Khomskii, *Transition Metal Compounds* (Cambridge University Press, 2004).
- [57] Huan Wang and Jing Wang, “Topological bands in two-dimensional orbital-active bipartite lattices,” *Phys. Rev. B* **103**, L081109 (2021).
- [58] Chen Fang, Matthew J. Gilbert, and B. Andrei Bernevig, “Bulk topological invariants in noninteracting point group symmetric insulators,” *Phys. Rev. B* **86**, 115112 (2012).
- [59] Y. Ikebe, T. Morimoto, R. Masutomi, T. Okamoto, H. Aoki, and R. Shimano, “Optical hall effect in the integer quantum hall regime,” *Phys. Rev. Lett.* **104**, 256802 (2010).
- [60] R. Shimano, G. Yumoto, J. Y. Yoo, R. Matsunaga, S. Tanabe, H. Hibino, T. Morimoto, and H. Aoki, “Quantum faraday and kerr rotations in graphene,” *Nature Commun.* **4**, 1841 (2013).
- [61] Ken N. Okada, Youtarou Takahashi, Masataka Mogi, Ryutaro Yoshimi, Atsushi Tsukazaki, Kei S. Takahashi, Naoki Ogawa, Masashi Kawasaki, and Yoshinori Tokura, “Terahertz spectroscopy on faraday and kerr rotations in a quantum anomalous hall state,” *Nature Commun.* **7**, 12245 (2016).
- [62] M. Mogi, Y. Okamura, M. Kawamura, R. Yoshimi, K. Yasuda, A. Tsukazaki, K. S. Takahashi, T. Morimoto, N. Nagaosa, M. Kawasaki, Y. Takahashi, and Y. Tokura, “Experimental signature of the parity anomaly in a semi-magnetic topological insulator,” *Nature Phys.* **18**, 390–394 (2022).
- [63] P. E. Blöchl, “Projector augmented-wave method,” *Phys. Rev. B* **50**, 17953–17979 (1994).
- [64] Stefan Grimme, Jens Antony, Stephan Ehrlich, and Helge Krieg, “A consistent and accurate ab initio parametrization of density functional dispersion correction (dft-d) for the 94 elements h-pu,” *J. Chem. Phys.* **132**, 154104 (2010).
- [65] A. A. Mostofi, J. R. Yates, Y.-S. Lee, I. Souza, D. Vanderbilt, and N. Marzari, “wannier90: A tool for obtaining maximally-localised wannier functions,” *Comput. Phys. Commun.* **178**, 685–699 (2008).
- [66] Q. Wu, S. Zhang, H.-F. Song, M. Troyer, and A. A. Soluyanov, “Wanniertools: An open-source software package for novel topological materials,” *Comput. Phys. Commun.* **224**, 405–416 (2018).
- [67] Jiacheng Gao, Quansheng Wu, Clas Persson, and Zhijun Wang, “Irvsp: To obtain irreducible representations of electronic states in the vasp,” *Comput. Phys. Commun.* **261**, 107760 (2021).
- [68] Atsushi Togo and Isao Tanaka, “First principles phonon calculations in materials science,” *Scr. Mater.* **108**, 1–5 (2015).
- [69] Shuichi Nosé, “A unified formulation of the constant temperature molecular dynamics methods,” *J. Chem. Phys.* **81**, 511–519 (1984).
- [70] Shuichi Nosé, “Constant Temperature Molecular Dynamics Methods,” *Prog. Theor. Phys. Supp.* **103**, 1–46 (1991).
- [71] William G. Hoover, “Canonical dynamics: Equilibrium phase-space distributions,” *Phys. Rev. A* **31**, 1695–1697 (1985).
- [72] Xu He, Nicole Helbig, Matthieu J. Verstraete, and Eric Bousquet, “Tb2j: A python package for computing magnetic interaction parameters,” *Comput. Phys. Commun.* **264**, 107938 (2021).
- [73] T. Ozaki, “Variationally optimized atomic orbitals for large-scale electronic structures,” *Phys. Rev. B* **67**, 155108 (2003).
- [74] T. Ozaki and H. Kino, “Numerical atomic basis orbitals from h to kr,” *Phys. Rev. B* **69**, 195113 (2004).
- [75] T. Ozaki and H. Kino, “Efficient projector expansion for the ab initio lcao method,” *Phys. Rev. B* **72**, 045121 (2005).
- [76] T. Holstein and H. Primakoff, “Field dependence of the intrinsic domain magnetization of a ferromagnet,” *Phys. Rev.* **58**, 1098–1113 (1940).
- [77] Ping Li, “Prediction of intrinsic two dimensional ferromagnetism realized quantum anomalous hall effect,” *Phys. Chem. Chem. Phys.* **21**, 6712–6717 (2019).
- [78] Qian Sui, Jiaxin Zhang, Suhua Jin, Yunyouyou Xia, and Gang Li, “Model hamiltonian for the quantum anomalous hall state in iron-halogenide,” *Chin. Phys. Lett.* **37**, 097301 (2020).
- [79] S. Mellaerts, R. Meng, V. Afanasiev, J. W. Seo, M. Houssa, and J.-P. Locquet, “Quarter-filled kane-mele hubbard model: Dirac half metals,” *Phys. Rev. B* **103**, 155159 (2021).